Symmetric time-division-multiplexed SQUID readout with two-layer switches for future TES observatories

Malcolm Durkin, Scott Backhaus, Simon R. Bandler, James A. Chervenak, Ed V. Denison, William B. Doriese, Johnathon D. Gard, Gene C. Hilton, Richard A. Lew, Tammy J. Lucas, Carl D. Reintsema, Daniel R. Schmidt, Stephen J. Smith, Joel N. Ullom, Leila R. Vale, Michael R. Vissers, Nicholas A. Wakeham

***Abstract*—Time-division multiplexing (TDM) of transition-edge-sensor (TES) microcalorimeters is being developed as the readout technology for the Athena X-ray integral field unit (X-IFU) and CMB-S4. We present an experimental demonstration of our latest TDM architecture, which has been implemented in a 4-column × 34-row chip that is fully compatible with the X-IFU design specifications. This new "mux21" architecture is designed for differential readout and uses two-layer switches to reduce the number of row-address lines while also incorporating changes that reduce power to roughly 40% and the total number of SQUIDs to half that of TDM chips used in previous publications. With the 160 ns row durations specified for X-IFU, we obtained (2.02 ± 0.03) eV FWHM energy resolution at 5.9 keV in 2-column × 34-row TDM readout of a NASA X-IFU-like TES array, which meets the requirements of X-IFU's energy-resolution budget. Finally, a scaling analysis of our improved TDM readout chain to bolometer applications indicates that multiplexing factors on the scale of several hundred are possible, depending on the readout requirements.**

***Index Terms*—transition-edge sensors, superconducting quantum interference devices, multiplexed readout, time-division multiplexing, Athena, X-IFU.**

I. Introduction

LARGE arrays of transition-edge sensors (TESs) have proliferated in microcalorimeter [1][2] and bolometer [3]-[7] applications due to the energy resolution and sensitivity offered by TESs. The scale of existing and future instruments necessitates the use of multiplexed readout. Time-division multiplexing (TDM) [8] is baselined for the X-ray integral field unit (X-IFU)[9], a several kilopixel array of TES X-ray microcalorimeters that is part of the ATHENA satellite mission, and is the preliminary baseline for CMB-S4 [10].

TDM is a high readiness TES readout technology that is routinely used in 250-pixel-scale microcalorimeter spectrometers [1] and kilopixel-scale bolometer arrays [3][4][7]. Improvements to TDM bandwidth [11] enabled 8-column x 32-row TDM of X-IFU-like TESs to achieve energy resolution of (2.16 ± 0.006) eV (FWHM) at 6.9 keV and (1.97 ± 0.01) eV at 5.9 keV [12], which met the X-IFU resolution and dynamic-range requirements with added engineering margins. Since these experiments, we have produced two new multiplexer designs, "mux20a" and "mux21".

Our "mux20a" design moved from a first-stage amplifier (SQ1) with four active SQUIDs to a SQ1 with two active SQUIDs. A reduction in the Josephson junction's area, and thus its capacitance, allowed the shunt resistances to double, which kept the SQ1 performance constant even with half the active elements. Further, simplification of the feedback to input coupling cancelation architecture [8] meant that mux20a used a total of four SQUID-like components (two active SQUIDs and two symmetrizing dummies) coupled to the SQ1 flux input transformer, compared to the 12 SQUID-like components (four active and eight dummies) of the previous mux19a chip, which resulted in a factor of 3 reduction in the areas of the SQ1 and SQ1 input transformer and a reduction in the total multiplexer area to 0.65x of the 2019 design. Additionally, the modifications we proposed in 2019 [11] yielded a 40% reduction in power dissipation compared to the 2019 design. With this new mux20a chip coupled to a new NIST SA20a SQUID series array amplifier (SSAA), we measured the full readout chain TO have 32-row multiplexed readout noise of 12.5 pA/√Hz referred to TES current at row durations (t_{row}) of 160 ns, which is equivalent to 185 $n\Phi_0$ / √Hz non-multiplexed and referred to SQ1 input flux. This is an improvement over the 306 $n\Phi_0$ / √Hz achieved in our 2018 40-row experiments [13] and 292 $n\Phi_0$ / √Hz achieved in the 2019 32-row experiments [12], which used legacy multiplexers and SA13 SSAAs. Two-layer switching [14] was also implemented in a mux20a variant to reduce the number of row address

Manuscript receipt and acceptance dates will be inserted here. The authors gratefully acknowledge funding from the NASA SAT program "Providing enabling & enhancing technologies for a demonstration model of the ATHENA X-IFU". *(Corresponding author: Malcolm Durkin.)*

M. Durkin and J. D. Gard are with University of Colorado, Boulder, CO 80309, USA (e-mail: malcolm.durkin@nist.gov, johnathon.gard@nist.gov).

S. Backhaus, E. V. Denison, W. B. Doriese, G. C. Hilton, T. J. Lucas. C. D. Reintsema, D. R. Schmidt, J. N. Ullom, L. R. Vale, and M. R. Vissers are with National Institute of Standards and Technology, Boulder, CO 80305, USA. (e-mail: william.doriese@nist.gov, joel.ullom@nist.gov).

S.R. Bandler, J. A. Chervenak, S. J. Smith, and N. A. Wakeham are with NASA Goddard Spaceflight Center, Greenbelt, MD 20771, USA (e-mail: simon.r.bandler@nasa.gov).

R. Lew is with Theiss Research, La Jolla, CA 92037, USA (e-mail: richard.lew@nist.gov).

Color versions of one or more of the figures in this paper are available online at http://ieeexplore.ieee.org.

Digital Object Identifier will be inserted here upon acceptance.

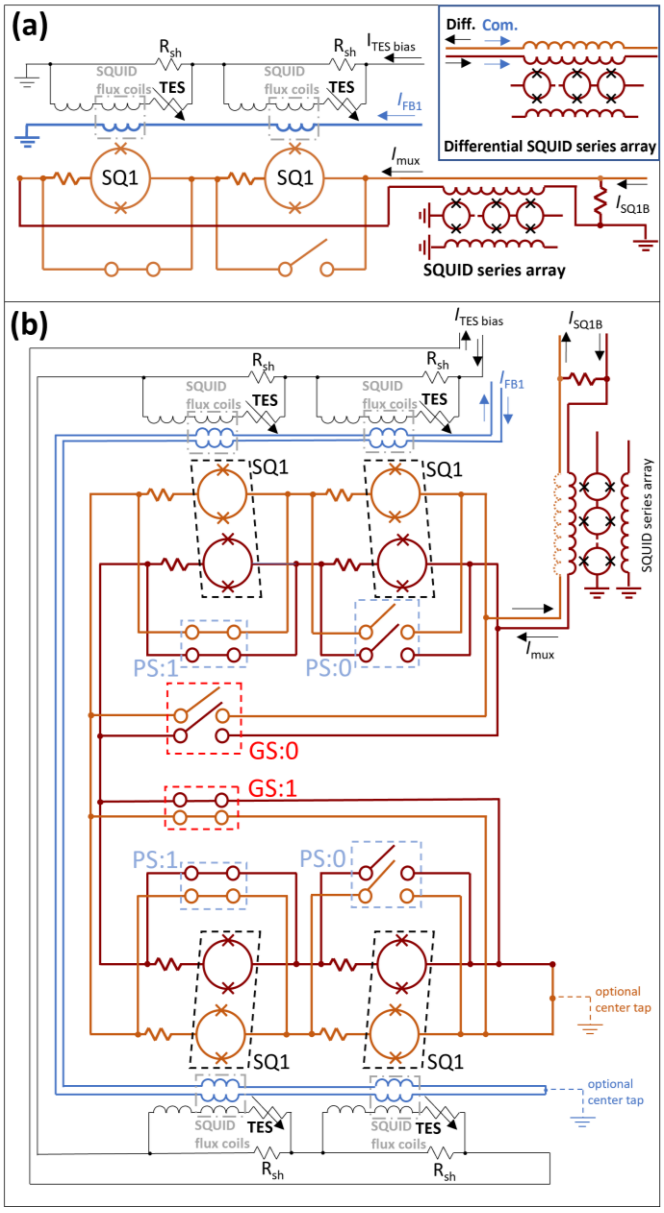

Fig. 1. (a) Circuit diagram of one-column x two-row single-ended TDM with single-layer row-address switches. Each TES's current is measured by a corresponding SQ1, which is activated by opening its corresponding superconducting switch. The current output the multiplexer is read out by a SQUID Series Array Amplifier. Inset: A differential series array can be used to reject a common-mode current signal on the multiplexer line. (b) Circuit diagram of one-column × four-row symmetric TDM for differential readout with two-layer switching. The SQ1 SQUIDs, resistors, and switch components are allocated evenly to identical TDM switching loops on either side of a symmetry point. Feedback coils are similarly divided across a symmetry point. For a SQ1 to be active, its corresponding GS and PS switches must both be open.

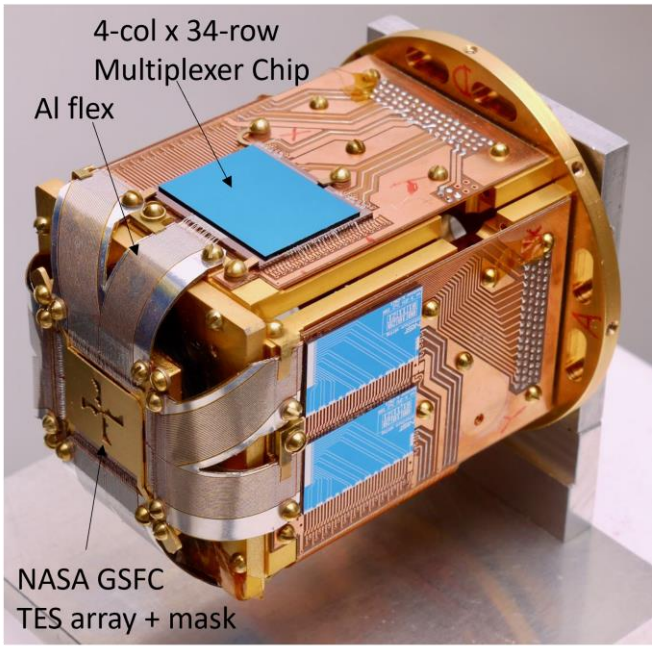

Fig. 2. NIST TDM snout with a 4-col × 34-row mux21 multiplexer chip and a NASA LPA 2.5a TES array. The multiplexer chip is cold-indium bump bonded to a carrier chip and interfaced to the TES array as it would be in X-IFU, but on a smaller scale. Each panel of the NIST TDM snout has wiring for only two TDM columns and the carrier chip connects 7 TES pixels to the multiplexer per column. A total of 14 pixels are read out using 2-column × 34-row readout, as all row address lines are connected.

lines and provided readout performance indistinguishable from that of a standard single-layer-switch mux20a.

Our most recent mux21 design combines the previous mux20a optimizations and two-layer switching with a new symmetrized multiplexer architecture that is compatible with symmetric-differential readout, which is baselined for X-IFU. The mux21 design has been implemented in two chip formats that integrate both the multiplexer and TES bias circuit components into their unit cells: a 6-pixel modular test chip and a large-format 4-column × 34-row X-IFU-like chip.

In this paper, we present the design and electrical testing of our mux21 architecture, including a 2-column x 34-row readout demonstration using an X-IFU-like TES array that achieves (2.02 ± 0.03) eV (FWHM) energy resolution at 5.9 keV. Additionally, we analyze how this state-of-the-art TDM readout architecture could increase the multiplexing factor in future arrays of TES bolometers.

II. Differential TDM Architecture

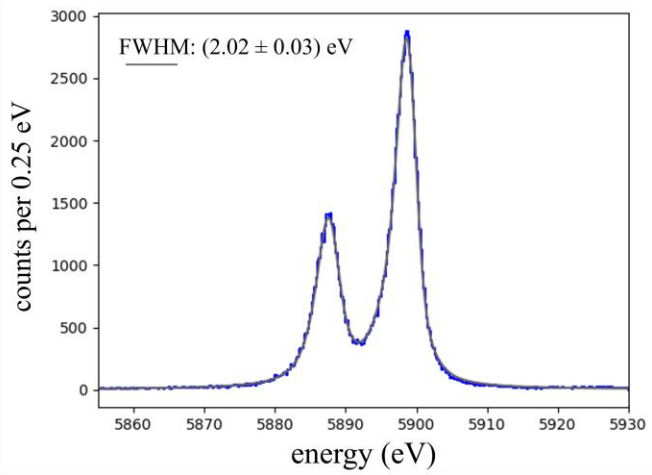

Fig. 3. Mn Kα spectrum using 2-column × 34-row TDM. Out of 14 connected TESs, one is excluded for being an outlier in TES pulse height.

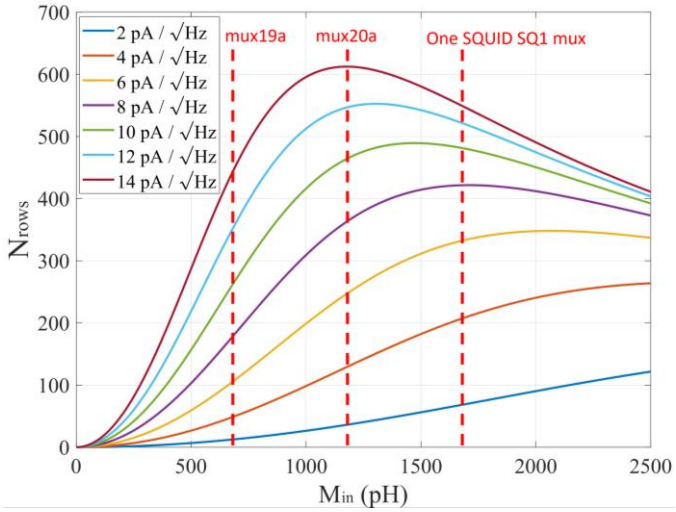

Fig. 4. The performance of a state-of-the-art TDM readout chain is scaled to bolometer applications, with the relationship between N_{rows} and M_{in} shown for several values of readout noise assuming $(dI_{TES}/dt)_{max}$ = 5.7 mA/s, $\sqrt{S_\Phi}$ = 185 nΦ_0 /√Hz, and t_{sett} = 109.5 ns. Vertical dashed lines indicate the predicted maximum M_{in} for L_{in} = 170 nH for mux19a (685 pH), mux20a (1186 pH), and a possible future multiplexer with a single SQUID per SQ1 (1679 pH).

TDM reads out TES currents sequentially within a multiplexing unit (column). In the modern switch-based TDM architecture [15], shown in Fig 1(a), each TES's current is measured as an input flux to its corresponding first stage SQUID ammeter (SQ1), which is activated by opening a corresponding superconducting flux-actuated switch (FAS)[16][17]. Within each column, SQ1s are activated one at a time, allowing the column's SQ1 current signals (I_{mux}) to be read out by a single readout chain consisting of a series array transimpedance amplifier (SSAA)[18] whose output voltage signal is read out by room-temperature electronics. Multiplexing factors as high as 40 have been demonstrated for microcalorimeters [13] and as high as 64 for bolometer experiments [3]. The scale of readout is increased further by operating many columns in parallel, with rows of flux switches sharing control lines. For X-IFU, prior to the ongoing 2022–2023 mission rescope, the planned TDM scale was 72-columns × 34-rows [9].

Symmetric-differential readout is baselined for X-IFU to reduce susceptibility to electromagnetic interference (EMI) [9]. The single-ended TDM circuit in Fig 1(a) is susceptible to common-mode pickup, because the SSAA input coil only measures one side of the multiplexer line. A second coil (shown in Fig. 1 (a) inset) would allow the flux from differential current signals to be added together and the flux from common-mode signals to be subtracted from one another, common-mode rejection. One difficulty in implementing such a symmetric scheme using the multiplexer in Fig. 1 (a) is that each multiplexer unit cell has parasitic capacitive coupling to the feedback, input, and FAS coils. Because these parasitic couplings can't be symmetrized for all active pixels, these lines will couple asymmetrically to the multiplexer circuit resulting in a differential component that will not be rejected by the differential series array.

Our latest multiplexer architecture, shown in Fig. 1 (b), achieves the needed symmetry by splitting each switching cell in two, dividing the SQ1 SQUIDs and FAS components evenly between switching loops on opposite sides of a symmetry point. The second layer of switching is divided similarly. Because the TES-current and feedback coils are coupled to SQUIDs and row-address coils are coupled to Zappe-SQUIDs [16] as identically as possible on either side of the symmetry point, capacitive coupling is designed to be perfectly symmetric. Additionally, the feedback coils are designed to reject common-mode signals in the same way splitting on either side of a symmetry point. Because each SQUID is still coupled to coils on both sides of the symmetry point, common-mode signals on the feedback line will be rejected.

Our mux21 4-column x 34-row chips use two-layer switching, which requires both a pixel select (PS) and a group select (GS) switch to be open to activate the corresponding SQ1. As shown in Fig. 1(b), each PS control line controls a pixel switch in every group of switches. This arrangement allows N_{rows} = N_{PS} × N_{GS} rows to be addressed, where N_{rows} is the total number of TDM rows, N_{PS} is the number of PS lines, and N_{GS} is the number of GS lines. The 34 rows in this chip are addressed via N_{GS} = 4 and N_{PS} = 9 (two of the 36 possible row-address combinations are not used).

Two-layer switching has been previously demonstrated [14] in quasi-static measurements of modular 11-channel chips. Unlike these first-generation chips, our recent designs (mux20a and later) have series resistors only in the innermost switching loop, as shown in Fig. 1(b). The second series resistor in the outer loop of the first-generation design increased the power dissipated by the multiplexer at 50 mK [14]. We have not observed any detrimental effects from the removal of the second resistor in the form of crosstalk or signal degradation; this is the expected behavior, due to the rapid settling times of the switch-loop currents and the absence of significant parasitic inductive coupling between the switch loops and the TES bias circuits.

III. 2-column × 34-row readout demonstration

Experimental measurements were performed in a NIST 8-column TDM system with 32 row address lines [1] and used a NASA LPA 2.5a TES array similar to one used in previous work [12][13]. As with the mux20a testing, the series arrays used here were also of the SA20a design. Similar to other NIST TDM systems, the readout is single-ended and significant modifications will be necessary to convert it to symmetric differential readout. As a result, these measurements demonstrate the performance and functionality of the multiplexer, while a full demonstration of differential readout is planned for future work. As pictured in Fig 2, the multiplexer chip is cold-indium bump bonded [20] to a wiring chip, which is connected to the TES chip via wirebonds to an aluminum flexible circuit. Each TDM column has seven TESs connected to multiplexer unit cells, but all 34 rows of SQ1s can be read out. In the 8x32 snout, each readout panel has wiring for only two columns, so we operate the 4-x34 multiplexer chip in a 2-column x 34-row configuration, reading out a total of 14 pixels. The duration of a row activation (t_{row}) is 160 ns, which matches the X-IFU specifications.

For X-ray measurements, the SQUIDs were flux locked at 30% of the combined (SQ1/SSAA) SQUID modulation depth from the top of the multiplexer I_{mux} vs SQ1 flux curve [11], with the output signal drifting towards the low I_{mux} side of the curve during the rising edge of the TES pulse as in previous demonstrations [12][13]. The 34-row multiplexed readout noise was 19 pA / √Hz referred to the TES with an input mutual inductance of 320 pH, which scales to 280 nΦ$_0$/√Hz non-multiplexed and referred to SQ1 flux. The noise degradation as compared to that achieved with mux20a (see Sec. I) is because the 4-column × 34-row chip's wafer had 28% lower SQ1 critical current (I_{cSQ1}) than the mux20a chips. A lower critical current lowers the gain of the SQ1 stage, which in turn increases the noise contributions of the subsequent SSAA and warm-amplifier stages. By contrast, the 6-pixel mux21 chips had only 8% lower I_{cSQ1} than the mux20a chips and achieved non-multiplexed readout noise of 212 nΦ$_0$ / √Hz referred to SQ1 flux. An X-ray spectrum was acquired from a fluoresced Mn source, with each TES receiving an average count rate of about 0.5 X-ray events per second. A coadded spectrum, shown in Fig. 3, yielded a best-fit FWHM energy resolution of (2.02 ± 0.03) eV at 5.9 keV. This result, which meets the requirements of X-IFU's energy-resolution budget, is achieved with a TDM chip that is fully compatible with all of X-IFU's packaging requirements.

IV. Scaling to Future Bolometer Missions

TDM is the preliminary baseline readout technology for CMB-S4, motivating its study for bolometer applications. Here, we scale the recent performance improvements to our TDM readout of TES microcalorimeters to the readout of slower TES bolometers. Repeating a past scaling analysis [21] but allowing some timing components of the row time to float, the noise of a TDM system is given by

$$\sqrt{S_A} = \frac{\sqrt{S_\Phi}}{M_{in}} \sqrt{N_{rows} \frac{(t_{sett} + t_{samp})}{t_{samp}}} \quad (1)$$

where $\sqrt{S_A}$ is the multiplexed readout noise referred to the TES current, $\sqrt{S_\Phi}$ is the non-multiplexed flux noise of the readout chain referred to SQ1, t_{sett} is the time allowed for settling during each row activation, t_{samp} is the time allocated to measuring the output of the readout chain during each row activation, and M_{in} is the input mutual inductance of the TES current to each SQ1 SQUID. The slew rate is constrained by

$$M_{in} \left(\frac{dI_{TES}}{dt} \right)_{max} \leq \alpha / t_{frame} \quad (2)$$

where $(dI_{TES}/dt)_{max}$ is the maximum TES current slew rate, $t_{frame} = N_{rows}\, t_{row} = N_{rows}\, (t_{sett} + t_{samp})$ is the frame time, and α is the maximum flux change between samplings that can be tracked by the flux locked loop algorithm. Most bolometer systems lock in the center of the SQUID curve (because input signals are equally likely to go up or down) where the most recent pulse tracking algorithms [22] allow $\alpha = 0.328\ \Phi_0$. Previously, with the canonical proportional-integral digital-feedback algorithm [8] $\alpha = 0.243\ \Phi_0$.

Fig. 4 shows the relationship between N_{rows} and M_{in} for different levels of white readout noise obtained by solving (1) and (2). A flux noise of 185 nΦ$_0$ / √Hz and a constant t_{sett} = 109.5 ns is assumed for a state-of-the-art TDM system, while $(dI_{TES}/dt)_{max}$ = 5.7 mA / s is taken from the 7.8 kHz frame rate and M_{in} = 685 pH of advanced ACTPOL [3]. t_{samp} varies as a function of M_{in}. The maximum M_{in} achievable is application dependent, with available multiplexer area and total self-inductance of the TES bias circuit being potential limitations. These restrictions are both relaxed when number of SQUIDs per SQ1 is reduced, with the impact of recent and possible reductions in SQUID numbers on maximum M_{in} for SQ1 input self-inductance (L_{in}) shown in Fig. 4.

The timing considerations are dependent on acceptable levels of time-forward crosstalk and the maximum allowed M_{in}. For any curve in Fig. 4, N_{rows} is maximized when $t_{sett} = 2\ t_{samp}$ for t_{row} =160 ns, corresponding to the shortest t_{row} and highest M_{in} that can be used without harming performance. Time-forward crosstalk is reduced as t_{row} is increased, but at a cost to N_{rows}. Fig. 5(a) shows experimental values of proportional time forward crosstalk, acquired by measuring the I_{FB1} offset in a flux locked row caused by a triangle I_{FB1} signal applied during the preceding row, and predicted reductions in N_{rows} compared to the maximum value for any curve in Fig. 4.

The value of t_{sett} = 109.5 ns was experimentally measured. The timing windows t_{sett} and t_{samp} are typically set by setting timings with digital electronics, $t_{samp,\ digital}$ and $t_{sett,\ digital}$. The values for scaling differ from the digital values due to bandwidth limits on the SQUID readout chain, which prolongs the effective t_{samp} and shortens the effective t_{sett}. Effective timings can be obtained by sweeping $t_{samp,\ digital}$ with a fixed digital settling time of $t_{sett,\ digital}$ = 128 ns, N_{rows} = 24, t_{row} = 480 ns, and padding the end of t_{row} with unused time. This holds the multi-

plexing factor from number of rows constant while allowing t_{sett} and t_{samp} dependencies to be studied. Noise measurements are shown in Fig. 5(b). A best-fit to our noise model finds t_{sett} = 109.5 ns, which is only incrementally different from the predicted optimal point of t_{sett} = 106.7 ns for 160 ns.

Two-layer switching makes larger multiplexing factors viable for kilopixel scale arrays. Each column requires four pairs of wires and each row address line requires one pair of wires from the 4 kelvin stage to the room-temperature electronics. As an example, a 1320-pixel TDM array would require 192 total signal lines for 33-col × 40-row single layer TDM and 197 lines for 8-col × 165-row single layer TDM, with the high-N_{row} option providing no advantage in wire count. By contrast, the same array could be read out with 58-lines using 8-col×13-GS×13-PS two-layer TDM, or roughly a factor of 3 reduction in wiring.

V. Conclusions

We used our most recent generation of TDM chips, which are compliant with X-IFU's packaging requirements, to measure energy resolution of (2.02 ± 0.03) eV (FWHM) at 5.9 keV in X-IFU-like TESs. Our scaling analysis indicates that the high bandwidth, reduced area, and two-layer switching of this TDM system for X-ray microcalorimeters could allow a multiplexing factor of up to several hundred TDM rows in future TES-bolometer applications.

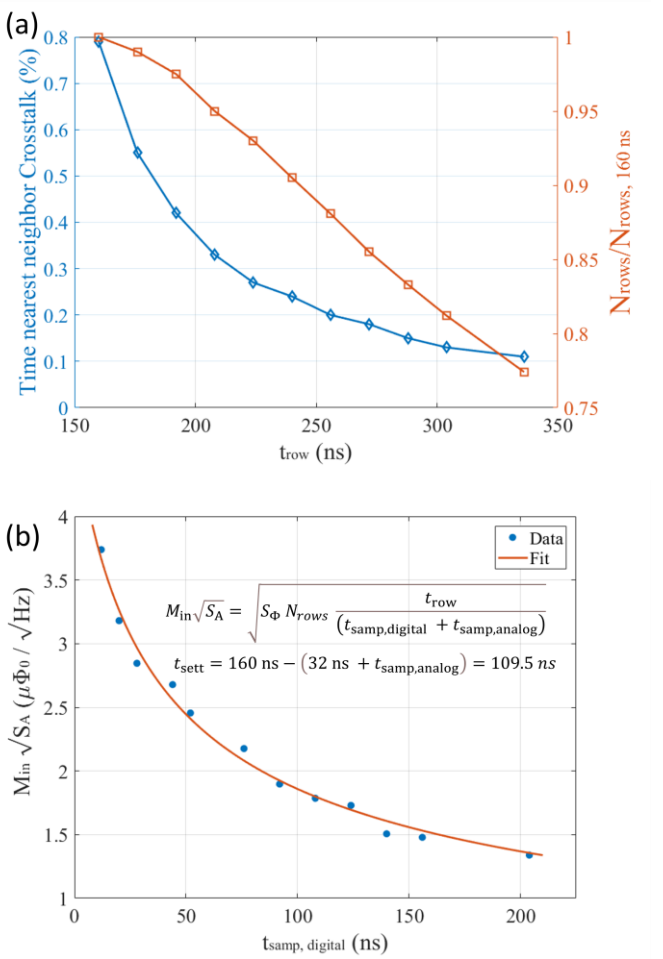

Fig. 5. (a) Time nearest neighbor crosstalk and decreases in Nrows as t_{row} is increased and t_{sett} is held constant. Since t_{samp} is being varied, crosstalk scales roughly as 1 / t_{samp}. Time nearest neighbor (TNN) crosstalk is determined by the bandwidth cutoff of the SQ1 feedback line. More drastic reductions in TNN crosstalk than shown can be accomplished by increasing Tsett or the bandwidth of the SQ1 feedback line. (b) Measured noise as $t_{samp,\ digital}$ is varied while other parameters are kept constant ($t_{sett,\ digital}$ = 128 ns, N_{rows} = 24, t_{row} = 480 ns). Equation (1) can be used to fit this plot with an additional free parameter, $t_{samp,analog}$, the effective contribution of the finite bandwidth of the SQUID readout chain to t_{samp}. This yields t_{sett} = 109.5 ns.

References

[1] W. B. Doriese *et al*., "A practical superconducting-microcalorimeter X-ray spectrometer for beamline and laboratory science," *Rev. Sci. Instrum.*, vol. 88, no. 5, pp. 053108-1-053108-23, Apr. 2017.

[2] J. N. Ullom and D. A. Bennett, "Review of superconducting transition-edge sensors for X-ray and gamma-ray spectroscopy," *Supercond. Sci. Technol.*, vol. 28, no. 8, pp. 084003, May 2015.

[3] S. W. Henderson *et al*., "Readout of two-kilopixel transition-edge sensor arrays for Advanced ACTPOL" *Proc. SPIE*, vol. 9914, pp. 99141G, July 2016.

[4] D. A. Harper *et al.*, "HAWC+, the Far-Infrared Camera and Polarimeter for SOFIA," JAI, vol. 7, pp. 1840008, June 2018.

[5] B. A. Benson *et al.*, "SPT-3G: a next-generation cosmic microwave background polarization experiment on the South Pole telescope," *Proc. SPIE*, vol. 9153, pp. 91531P, July 2014.

[6] N. Galitzki *et al*., "The Simons Observatory: instrument overview," *Proc. SPIE*, vol. 10708, pp. 1070804, July 2018.

[7] W. Holland *et al*., "SCUBA-2: a 10,000-pixel submillimeter camera for the James Clerk Maxwell Telescope," *Proc. SPIE*, vol. 6275, pp. 62751E, July 2013.

[8] P. A. J. de Korte *et al*., "Time-division superconducting quantum interference multiplexer for transition-edge sensors," Rev. Sci. Instrum., vol. 4, no. 8, pp. 3807-3815, Aug. 2003.

[9] H. Geoffray *et al*., "Design of the detection chain for Athena X-IFU," *Proc. SPIE*, vol. 12181, pp. 121810M, Aug. 2022.

[10] K. Abazajian et al., "CMB-S4 Science Case, Reference Design, and Project Plan" arXive:1907.04473, July 2019.

[11] M. Durkin *et al*., "Mitigation of finite bandwidth effects in time-division-multiplexed SQUID readout of TES arrays," *IEEE Trans. Appl. Supercond.*, vol. 31, no. 5, Aug. 2021, Art. No. 1600905.

[12] S. J. Smith *et al*., "Performance of a broad-band, high resolution, transition-edge spectrometer," *IEEE Trans. Appl. Supercond.*, vol. 31, no. 5, Aug. 2021, Art. No. 2100806.

[13] M. Durkin *et al*., "Demonstration of Athena X-IFU compatible 40-row time-division-multiplexed readout," IEEE Trans. Appl. Supercond., vol. 29, No. 5, Aug. 2019, Art. No. 2101005.

[14] C. S. Dawson *et al*., "Two-level switches for Advanced time-division multiplexing," *IEEE Trans. Appl. Supercond*., vol. 29, no. 6, Aug. 2019, Art. No. 2500205.

[15] W. B. Doriese *et al*., "Developments in time-division multiplexing of X-ray transition-edge sensors," *J. Low Temp. Phys*., vol. 184, no. 1/2, pp. 389-395, Jul. 2016.

[16] H.H. Zappe, "Josephson quantum interference computer devices," *IEEE Trans. Magn.*, vol.13, no. 1, pp.41-42, Jan. 1977.

[17] J. Beyer and D. Drung, "A SQUID multiplexer with superconducting-to-normalconducting switches," *Supercond. Sci Technol*., vol 21, no.10, Oct. 2008, Art. No. 105022.

[18] R. P. Welty and J. M. Martinis, "Two-stage integrated SQUID amplifier with series array output," IEEE Trans. Appl. Supercond. Vol. 3, no. 1, pp.2605-2608, Mar. 1993.

[19] C. T. Chantler, M. N. Kinnane, C.H. Su, and J. A. Kimpton, "Characterization of Kα spectral profiles for vanadium component redetermination for scandium titanium chromium and manganese and development of satellite structure for Z = 21 to Z = 25," *Phys. Rev. A*, vol. 73, no. 1, Jan. 2006.

[20] T. J Lucas *et al.*, "Indium Bump Process for Low-Temperature Detectors and Readout," *J. Low Temp. Phys.*, pp. 1-6, Mar. 2022.

[21] W. B. Doriese *et al*., "Optimization of TES-bias circuit for a multiplexed microcalorimeter array," *J. Low Temp. Phys.*, vol. 167, pp. 595-601, Jan. 2012.
[22] M. Durkin *et al*., "A predictive control algorithm for time-division-multiplexed readout of TES microcalorimeters," *J. Low Temp. Phys.*, vol. 199, pp. 275-280, Jan. 2020.